Separation and Purification Technology 309 (2023) 122878

Contents lists available at ScienceDirect

Separation and Purification Technology

journal homepage: www.elsevier.com/locate/seppur

Combination of genetic algorithm and CFD modelling to develop a new model for reliable prediction of normal shock wave in supersonic flows contributing to carbon capture

Seyed Heydar Rajaee Shooshtari [a], Jens Honoré Walther [b,c], Chuang Wen [d,*]

[a] Department of Chemical Engineering, Faculty of Engineering, Ferdowsi University of Mashhad, Mashhad, Iran
[b] Department of Civil and Mechanical Engineering, Technical University of Denmark, DK-2800 Kgs. Lyngby, Denmark
[c] Computational Science and Engineering Laboratory, ETH Zürich, CH-8092 Zürich, Switzerland
[d] Faculty of Environment, Science and Economy, University of Exeter, Exeter EX4 4QF, UK

ARTICLE INFO

Keywords:
Carbon capture
Supersonic separator
Genetic algorithm
CFD
Shock wave
Supersonic separation

ABSTRACT

Carbon dioxide separation and capture using green and efficient methods is an important issue in studies related to climate change. The supersonic separator is one of the efficient and reliable methods that can be used to separate impurities, including carbon dioxide, from gas streams. Reliable estimation of normal shock wave position plays a vital role in the proper design and simulation of supersonic separators. Many studies have used a one-dimensional theoretical (ideal) model of a normal shock wave for the estimation of the shock position and pressure recovery, but the accuracy of the ideal model of normal shock may be insufficient in some situations, as reported in the literature. A novel approach is presented in this paper to provide new equations for normal shock waves by the combination of computational fluid dynamics (CFD) and genetic algorithm. The comparison of the proposed model with several experimental data and the ideal model of a normal shock wave indicate that the present model provides more accurate predictions than the traditional model of a normal shock wave. The present model showed an average absolute relative deviation (*AARD*) of 1.80%, which is about six times less than *AARD* of the ideal model, indicating the robustness of the proposed model. Consequently, the present model can be employed as an accurate and efficient tool for the prediction of shock position and design of converging–diverging nozzles.

1. Introduction

Carbon dioxide (CO_2) constitutes a major part of greenhouse gas emissions to the atmosphere that can have adverse environmental effects and climate change [1]. Carbon capture and storage (CCS) is considered as an innovative technology for reducing CO_2 emissions [2]. There are several industrial methods that are mainly used for CO_2 removals, such as chemical and physical absorption, adsorption, membrane separation and cryogenic process. These technologies have high energy consumption, high capital and operating investment, large facilities and low CO_2 recovery rates [3].

The supersonic separator is one of the newest and most efficient methods among various techniques for CO_2 capture [4–6]. It can also be used for dehydration of natural gas and hydrocarbon dew point correction [7], H_2S removal [8,9], air pre-purification [10] and LNG production [11]. The supersonic separator consists of a swirling device, a converging–diverging nozzle, a liquid collection point and a pressure recovery section [12], as shown in Fig. 1. The design of the supersonic separator should be such that the shock wave occurs at the beginning of the pressure recovery section, to prevent droplets vaporization and obtain suitable pressure recovery.

The proper adjustment of the shock position in a supersonic separator is of particular importance. If the shock position is adjusted before the liquid collection point, the condensed droplets will be evaporated. On the other hand, locating the shock position very far from the liquid collection point can decrease pressure recovery and increase energy loss. Due to the significant importance of the normal shock in the pressure recovery section of supersonic separators, some researchers focused on this subject in the literature.

Jassim et al. [13] investigated the shock wave position in the supersonic nozzle for the real and ideal gas conditions by computational

* Corresponding author.
E-mail address: c.wen@exeter.ac.uk (C. Wen).

https://doi.org/10.1016/j.seppur.2022.122878
Received 16 October 2022; Received in revised form 23 November 2022; Accepted 5 December 2022
Available online 15 December 2022

Nomenclature

Symbols

A	cross sectional area (m^2)
a^*	low-Reynolds number correction (-)
a_1	constant (0.31)
a_m	Peng-Robinson parameter (m^6 Pa kg^{-2})
b_m	Peng-Robinson parameter (m^3 kg^{-1})
B_1	Peng-Robinson parameter (-)
B_2	Peng-Robinson parameter (m^3 kg^{-1})
C	constant (-)
C_p	specific heat at constant pressure (Pa m^3 kg^{-1} K^{-1})
d_e	hydraulic diameter
E	total energy (J kg^{-1})
F	blending function (-)
f	friction factor (-)
h	enthalpy (J kg^{-1})
k	turbulent kinetic energy (J kg^{-1})
$\dot{m}_t$	total mass flow rate (kg s^{-1})
Ma	Mach number (-)
P	gas pressure (Pa)
PR	pressure ratio (-)
R	gas constant (Pa m^3 kg^{-1} K^{-1})
T	gas temperature (K)
u	gas velocity (m/s)
X	process variable (-)
$\widetilde{X}$	normalized value (-)
x	axial direction (-)
Z	square of Mach number (-)

Greek letters

α	Peng-Robinson parameter (-)
γ	specific heat ratio (-)
ρ	gas density (kg m^{-3})
δ_{ij}	Kronecker delta (-)
λ_{eff}	effective heat conductivity (W/m K^{-1})
τ_{ij}	viscous stress (N/m^{-2}(−|-))
μ	dynamic viscosity (Pa s)
ω	specific dissipation rate (s^{-1})
Ω	strain rate magnitude (s^{-1})
ν	specific volume (m^3 kg^{-1})

Subscripts

0	Stagnation condition
eff	effective
tu	turbulent
e	exit
t	throat
in	inlet
min	minimum
max	maximum
i	ideal
u	upstream
d	downstream
G	gas

fluid dynamics (CFD) simulation. In another work [14] they studied the relationship between the position of shock and geometry of the nozzle and vorticity. Malyshkina [15] investigated the behaviour of gas in the region of a normal shock wave in a supersonic separator unit using two-dimensional compressible Euler equations. Karimi and Abdi [16] examined the influence of inlet and outlet conditions on the shock position in a Laval nozzle. Wen et al. [17,18] studied the effects of the shock wave position on the temperature distribution in a supersonic separator. Furthermore, they reported that the conical diffuser provides suitable pressure recovery for the supersonic separator.

Castier [19,20] presented a one-dimensional steady-state model for supersonic nozzles with and without side streams. The shock position was obtained in his work using the one-dimensional mass, energy and momentum balances across the shock wave. Yang et al. [21] studied the effects of various equations of state on the normal shock position in the supersonic separator using CFD simulation. In another work [22] they compared the results of the theoretical equations of normal shock with the CFD simulation results. Shooshtari and Shahsavand [23] studied the maximum pressure recovery in supersonic separators via a combination of condensation and normal shock waves. Furthermore, they investigated the pressure recovery for the case where heterogeneous condensation occurs in the supersonic separator unit [24].

Cao and Yang [25] experimentally investigated the dehydration performance and pressure recovery coefficient of a newly designed supersonic separator. In their work, an ellipsoidal central body was used to decrease gas flow resistance.

Bian et al. [26] improved the structure of the supersonic separator unit by investigating the effects of pressure ratio on the position of a normal shock wave. Secchi et al. [27] proposed a primary design for heavy hydrocarbon separation from natural gas streams using supersonic separators. Niknam et al. [28] proposed a model to control the supersonic separation units against disturbances in the inlet pressure and composition. Furthermore, they proposed an artificial neural network model for the prediction of the shock wave location inside Laval nozzles [29].

Jassim [30] investigated the effects of nozzle shape on pressure recovery and separation efficiency during the natural gas dehydration process. Alnoush and Castier [31] proposed a shortcut one-dimensional model of natural gas supersonic separation. Majidi and Farhadi [32] investigated the effect of operational parameters on the shockwave position. Wen et al. [33] and Cao et al. [34] studied the fluid flow inside a supersonic separator unit using the combination of non-equilibrium condensation and normal shock wave phenomena. Liu et al. [35] focused on boundary layer separation behind a shock wave in the supersonic Laval nozzle.

According to the mentioned literature review above, the studies carried out regarding the use of the normal shock wave for pressure recovery purposes in supersonic nozzles or supersonic separators can be classified into several aspects. Many researchers have studied the effects of operating conditions and nozzle geometry configurations on the normal shock wave position. Some articles have investigated the appropriate conditions for natural gas dehydration and heavy hydrocarbon separation by the supersonic separator in the presence of a normal shock wave. Another category of studies has investigated the simultaneous effects of the normal shock wave and condensation on the flow behaviour in supersonic nozzles. A number of studies have also focused on the maximization of pressure recovery inside supersonic separators.

The studies mentioned above can be also classified into two categories from the point of view of modelling and simulation. Some studies have used commercial software such as FLUENT to simulate the flow inside the nozzle in the presence of a normal shock wave.

Some of the studies mentioned have used a one-dimensional theoretical (ideal) model of a normal shock wave for the estimation of the shock position and pressure recovery [10,12,16,19,20,23,24,27,31]. However, the accuracy of the ideal model of a normal shock wave is

limited and the values predicted by this model are significantly different from experimental results in some situations and conditions, as reported in the literature. For example, Papamoschou et al [36] experimentally investigated the effects of nozzle pressure ratios on the shock position in planar nozzles. They reported that there is a significant difference between the actual position of normal shock and the position predicted by one-dimensional theory. In another research, Jassim and Awad [37] investigated the influence of the nozzle shape on the shock wave in the supersonic nozzle for natural gas processing. They also showed that the shock wave location predicted by one-dimensional approximation is widely far from the experimental data, especially at high nozzle pressure ratios (NPRs).

Furthermore, the normal shock wave also occurs inside the ejector and some theoretical studies about the ejector system have also used the one-dimensional model of the normal shock wave [38–40].

Although the one-dimensional model cannot accurately predict the shock wave location in some situations, its simplicity and ease of use made it used in many studies. The main innovation of the current study is to improve the accuracy of the one-dimensional model of the normal shock wave so that the model is both simple and more accurate.

Therefore, the present study aims to propose a new model for the reliable prediction of pressure ratio across the normal shock wave in the convergent-divergent nozzle by the combination of computational fluid dynamics and genetic algorithm. The suggested model will be compared to experimental data and the one-dimensional theoretical model of a normal shock wave.

2. Mathematical procedures

In the present study, the combination of CFD and genetic algorithm is used to propose a model that allows for predictions regarding the pressure ratio across the normal shock wave. For this purpose, a set of data are generated in the present study by two-dimensional simulation of compressible flow in axisymmetric and planar converging- diverging nozzles. These data set are used to propose an equation for the normal shock pressure ratio with the help of genetic algorithm.

2.1. Data generation using CFD

In order to provide a new and comprehensive model for the normal shock wave, a large amount of experimental data is required in a wide range of operating conditions and compositions, which is not currently available in the literature. Hence one hundred data are generated using the ANSYS FLUENT CFD software, in a wide range of inlet conditions and nozzle geometry configurations. This section details the data generation process and the CFD procedure performed in the current study such as governing equations, turbulence model, equation of state and numerical procedure.

2.1.1. Governing equations

The governing equations are the continuity, the momentum and the energy equations. Assuming steady state condition, the gas phase equations can be expressed as [41]:

$$\frac{\partial}{\partial x_i}(\rho u_i) = 0 \tag{1}$$

$$\frac{\partial}{\partial x_j}\left(\rho u_i u_j + P\delta_{ij} - \tau_{ji}\right) = 0 \tag{2}$$

$$\frac{\partial}{\partial x_j}\left(\rho u_j E + u_j P + \lambda_{eff}\frac{\partial T}{\partial x_j} - u_i \tau_{ij}\right) = 0 \tag{3}$$

where P,ρ, u,δ_{ij}, λ_{eff} and T are the gas pressure, the gas density, the gas velocity, the Kronecker delta, the effective heat conductivity and the gas temperature. E is the total energy consists of gas sensible enthalpy, pressure energy, and kinetic energy. τ_{ij} is the viscous stress and can be obtained via the following equation [41,42]:

$$\tau_{ij} = \mu\left[\left(\frac{\partial u_i}{\partial x_j} + \frac{\partial u_j}{\partial x_i}\right) - \frac{2}{3}\mu_{eff}\frac{\partial u_l}{\partial x_l}\delta_{ij}\right] \tag{4}$$

where μ is the dynamic viscosity of the fluid and μ_{eff} is the effective turbulent viscosity, which is the summation of the dynamic viscosity and the turbulent viscosity ($\mu_{eff} = \mu + \mu_{tu}$).

2.1.2. Turbulence model

The turbulence model plays an important role in precise modeling of the flow inside the Laval nozzle. It can also have a significant effect on accurate prediction of normal shock position and pressure recovery. The shear stress transport (SST) k-ω turbulence model is used here because of its suitable predictions for supersonic flows [42,43]. The following equations provide the turbulent kinetic energy (k) and the specific dissipation rate (ω) equations in SST model [41]:

$$\frac{\partial}{\partial t}(\rho k) + \frac{\partial}{\partial x_i}(\rho k u_i) = \frac{\partial}{\partial x_j}\left(\Gamma_k \frac{\partial k}{\partial x_j}\right) + \bar{G}_k - Y_k + S_k \tag{5}$$

$$\frac{\partial}{\partial t}(\rho \omega) + \frac{\partial}{\partial x_j}(\rho \omega u_j) = \frac{\partial}{\partial x_j}\left(\Gamma_\omega \frac{\partial \omega}{\partial x_j}\right) + \bar{G}_\omega - Y_\omega + D_\omega + S_k \tag{6}$$

The turbulent viscosity μ_{tu} is a function of kinetic energy and specific dissipation rate and can be computed by the following equation [42].

$$\mu_{tu} = \frac{\rho k}{\omega}\frac{1}{\max\left[\frac{1}{a^*}, \frac{\Omega F}{a_1 \omega}\right]} \tag{7}$$

where Ω is the strain rate magnitude, a^* is the low-Reynolds number correction, a_1 is a constant ($a_1 = 0.31$) and F is the blending function.

2.1.3. Equation of state

Using the appropriate equation of state is also important in this system to determine the position of shock and the shock pressure ratio. The Peng-Robinson equation of state is employed in this study to relate temperature, pressure and density of the gas phase in the Laval nozzle. This equation is widely used in studies of supersonic separator [31] and can be expressed as:

$$P = \frac{RT}{v - b_m} - \frac{a_m \alpha}{v(v + b_m) + b_m(v - b_m)} \tag{8}$$

where v is the specific volume, R is the gas constant, a_m, α are b_m are the Peng-Robinson parameters and can be computed according to mixing rules [16].

2.1.4. Numerical schemes

Numerical simulations are performed in ANSYS FLUENT 2020 R2 software. The density-based scheme is used to solve the compressible flow and the second order upwind scheme is employed to discretize the governing equations. The convergence criterion is set to 1×10^{-6} for all equations. In all simulations, the grid independence was tested to ensure that the results are independent to the size of meshes. The pressure

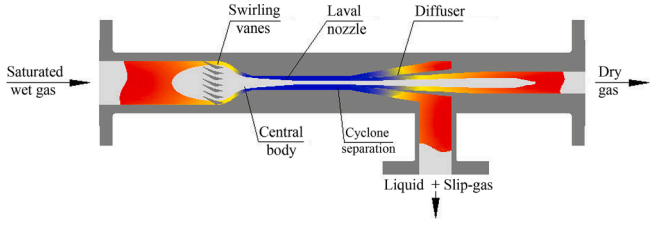

Fig. 1. Schematic diagram of a typical supersonic separator [18].

Table 1
The range of area ratios of Laval nozzles and operating conditions used in simulations.

Parameters	symbol	Unit	Values
Nozzle area ratio	A_e/A_t	–	1.2–4.3
Cross sectional shape of nozzle	–	–	Rectangle and Circle
Specific heat ratio (for different working fluids)	γ	–	1.13–1.66
Inlet pressure	P_{in}	MPa	0.1 – 8
Inlet temperature	T_{in}	K	273 – 340

boundary conditions are defined for both ends of the converging–diverging nozzle. Furthermore, for the walls of nozzle, no-slip and adiabatic boundary conditions are applied.

2.1.5. Data generation

As mentioned earlier, one hundred simulations with different conditions and different nozzle geometry configurations were performed using FLUENT software to create the data needed for model training. The range of operating conditions and the range of Laval nozzle area ratios used in simulations are shown in Table 1.

For example, Fig. 2 illustrates the pressure contour and the centerline pressure distribution along the Laval nozzle with $A_e/A_t = 1.21$. The inlet stagnation pressure and temperature of this simulation are 3 MPa and 300 K, respectively. Based on the simulation results, the pressure ratio at the shock location can be estimated. For other simulations, the same procedure was also used to complete the data generation process.

It should be noted that the specific heat ratio is included in Table 1 due to its importance and impact on the normal shock wave, as have been investigated by Yang et al. [22]. This physical property has a direct effect on the speed of sound and the Mach number.

After various investigations, it was found that the pressure ratio obtained from CFD results at the shock position (PR_{CFD}) can be achieved as a function of ideal pressure ratio (PR_i, which will be described in equation (10)), inlet stagnation pressure (P_0) and the specific heat ratio of the fluid (γ). The variable controlling method was used to assess the effects of the influencing factors on the normal shock pressure ratio. For this purpose, the effect of changing one parameter was investigated while other variables were held constant.

In the data generation process, when the input and output variables have different ranges, the entire data set should be normalized to avoid inconsistencies in data. Therefore in the current study, the created data sets are initially normalized using equation (9) to avoid differences in the magnitude order of variables.

$$\widetilde{X} = \frac{X - X_{\min}}{X_{\max} - X_{\min}} \tag{9}$$

here X is the actual value of the process variable, $\widetilde{X}$ is the normalized value of X, subscripts min and max denote minimum and maximum parameter values, respectively.

2.2. Model description and objective function

As mentioned in the previous sections, the main purpose of the present study is to provide a reliable equation to predict the pressure ratio across a normal shock wave. In the gas dynamics, the following theoretical (ideal) equation can be used to estimate the normal shock wave pressure ratio [22]:

$$PR_i = \frac{2\gamma Ma_u^2 - \gamma + 1}{\gamma + 1} \tag{10}$$

where PR is the pressure ratio, Ma is the Mach number and the subscript i is the ideal (theoretical) state and subscript u is the upstream location of the shock wave. As mentioned earlier, previous studies have shown that a comparison of the experimental data with the results of equation (10) shows that this equation fails to accurately predict the pressure ratio across the normal shock in some situations, especially for higher

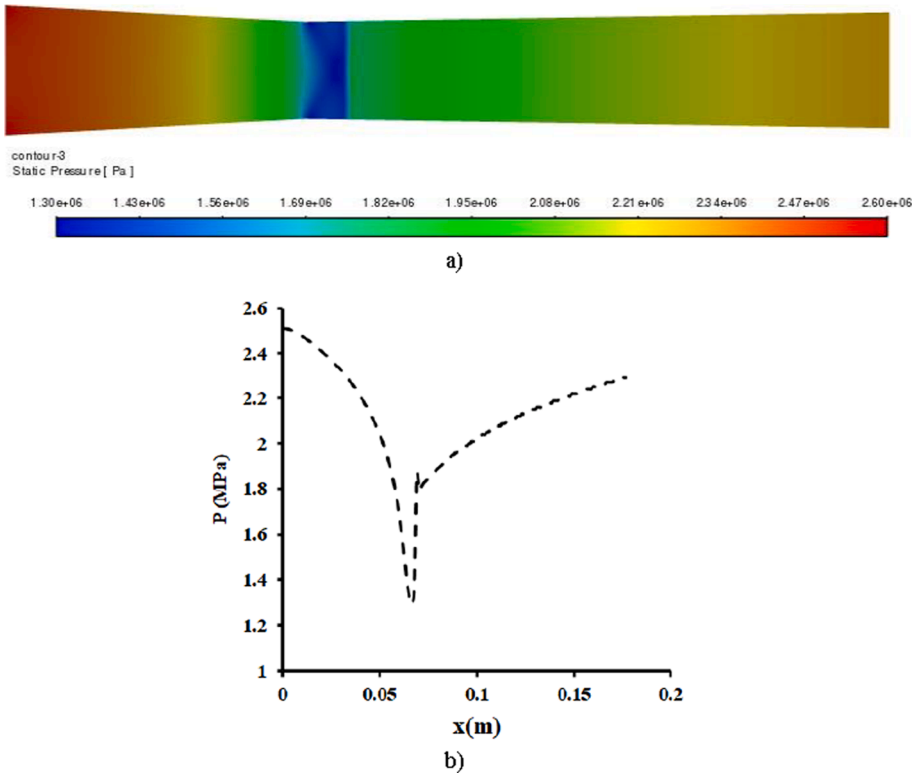

Fig. 2. Pressure distribution in the Laval nozzle: a) contours; b) pressure along the centerline.

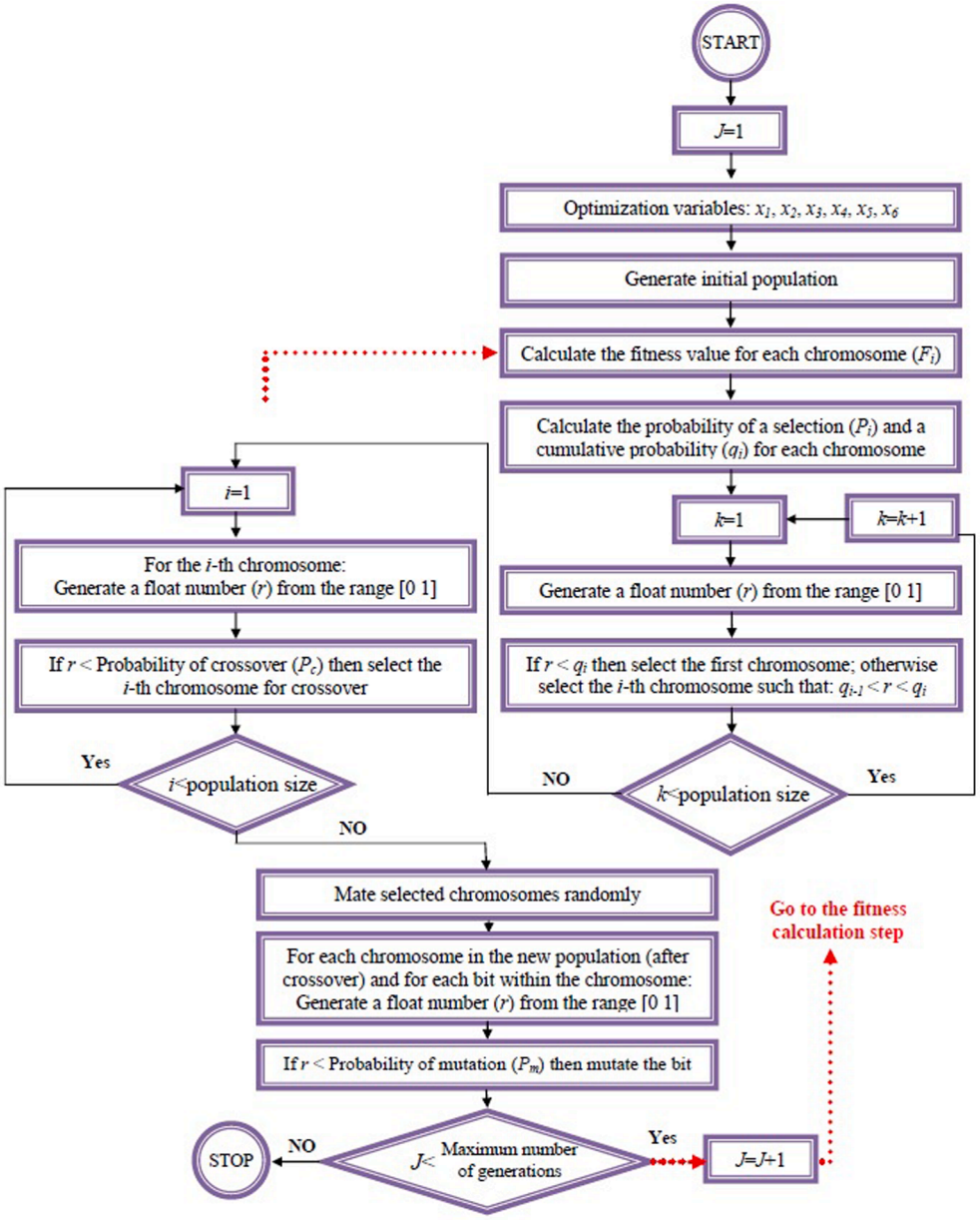

Fig. 3. The procedure of the genetic algorithm used in this study.

values of the expansion ratios (A_e/A_t) [36,37]. The reason behind this may be due to neglecting the effects of turbulence and equation of state on the normal shock pressure ratio.

In this work, we modify the theoretical equation of normal shock pressure ratio by using two Gaussian correction factors as below:

$$\widetilde{PR} = \eta_1 \eta_2 \widetilde{PR}_i \tag{11}$$

$$\eta_1 = x_1 \exp\left(- \left(\frac{\tilde{\gamma} - x_2}{x_3} \right)^2 \right) \tag{12}$$

$$\eta_2 = x_4 \exp\left(- \left(\frac{\widetilde{P_0} - x_5}{x_6} \right)^2 \right) \tag{13}$$

where $\sim$ denotes the normalized value, P_0 is the inlet stagnation pressure in Pa and x_1 to x_6 are constant coefficients that need to be determined according to the information obtained from the CFD simulations.

The unknown parameters in equations (12) and (13) are optimized in order to obtain the best fit to the CFD data. The objective function (f) is the sum of squared error (SSE) between the CFD data and the model predictions and is defined as follows:

$$f = \sum_{k=1}^{n} \left(\widetilde{PR}_{CFD,k} - \widetilde{PR}_k \right)^2 \tag{14}$$

where n is the number of data points.

The minimization of the objective function is done using the Genetic Algorithm (GA) which will be described in the next section. Furthermore, for a better comparison between the model results and CFD data, three statistical parameters including the root mean square error ($RMSE$), the average absolute relative deviation ($AARD$) and the coefficient of determination (R^2) are computed by the equations (15), 16 and 17, respectively.

$$RSME = \left(\frac{1}{n} \sum_{k=1}^{n} \left(PR_{CFD,k} - PR_k \right)^2 \right)^{0.5} \tag{15}$$

Table 2
Genetic algorithm parameters used in this study.

Parameter	Value
Maximum number of generations	100,000
Accuracy	0.0001
Population size	20
Crossover rate	0.25
Mutation rate	0.01

$$AARD\,(\%) = \frac{100}{n}\sum_{k=1}^{n}\left|\frac{PR_{CFD,k} - PR_k}{PR_{CFD,k}}\right| \quad (16)$$

$$R^2 = 1 - \frac{\sum_{k=1}^{n}\left(PR_{CFD,k} - PR_k\right)^2}{\sum_{k=1}^{n}\left(PR_{CFD,ave} - PR_k\right)^2} \quad (17)$$

2.3. Genetic algorithm

A genetic algorithm program is written using MATLAB to find the optimal model parameters. This method is based on the Darwin's theory of evolution and consists of various genetic operators such as selection, mutation and crossover [44]. In this method, each possible solution is encoded by binary strings referred to as a chromosome. So, each chromosome consists of bits (0 and 1) and these bits are called genes. At first, the initial population should be generated randomly, then, the fitness value of each chromosome is estimated. Afterward, the new population is created by selection operator which the individuals are chosen based on their fitness values. In the present study, the roulette wheel method is used for selection purpose. The next step is crossover which the pairs of strings is combined to create new strings (chromosome) with a new fitness value. It is likely that the new strings have better fitness values than each of their parents. The final stage is mutation which some bits are changed, randomly. It should be noted that the individuals are more likely to be selected for cross over and mutation processes which have better fitness values. The flowchart of the GA used in this study is shown in Fig. 3. Furthermore, the values of the parameters of the GA code are illustrated in Table 2.

3. Propose a new model

The purpose of this study is to find a new model for prediction of pressure ratio across the normal shock wave. The optimal parameters of the proposed model (equation (11)) are reported in Table 3. As mentioned earlier, three statistical parameters including AARD, RMSE and R^2 are used to evaluate the accuracy of the model. According to the statistical parameters in the Table 3, the proposed model has good agreement with CFD data sets.

The final form of the model can also be derived based on the equations (9), 11, 12 and 13 and based on the values given in Table 3:

$$PR = (C_1 PR_i + C_2)\exp\left(-(C_3\gamma + C_4)^2\right)\exp\left(-(C_5 P_0 + C_6)^2\right) + C_7 \quad (18)$$

The constants of this equation are also given in Table 4. Furthermore,

Table 5
The ANOVA table for multiple regression (equation (18)).

Source of variation	Degrees of freedom	Sum of squares	Mean sum of squares	F-ratio
Regression (model)	3	146.36	48.79	812.08
Error (residuals)	96	5.77	0.06	–
Total	99	127.77	1.29	–

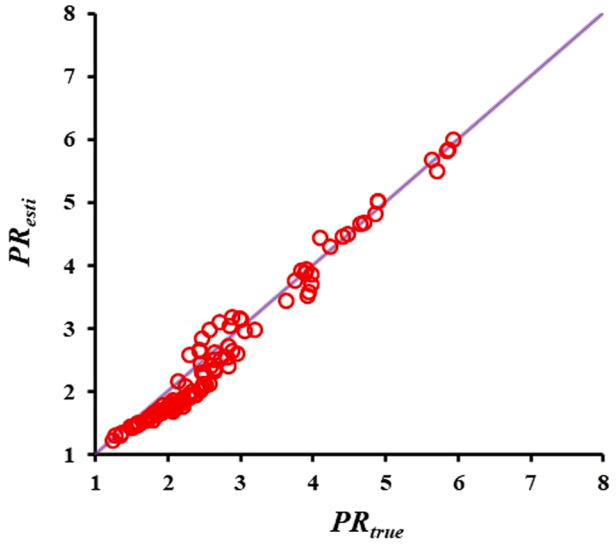

Fig. 4. The plot of true values (from CFD) vs estimated values (from the present model) for the pressure ratio across the shock.

the ANOVA (analysis of variance) table for equation (18) is shown in Table 5.

It should be noted that in the equation (18), all variables are dimensionless except for P_0 which is in Pascal.

In order to better evaluate the accuracy of the proposed model, a comparison between the predicted and CFD results is shown in Fig. 4. As can be seen, good agreement is obtained between the predictions of model and CFD values and a tight cloud of points about 45° line indicate the robustness of the new model.

It should be noted that as can be seen in Fig. 4, the results predicted by the model deviate slightly from the generated data at low pressure ratio values. In order to increase the accuracy of the predictions for low-pressure ratio of the normal shock ($PR_i < 2.3$), the constants presented in Table 6 can be used. The method of obtaining these constants is similar to the previously mentioned approach. Therefore, the constants presented in Table 4 can be used for all pressure ratio ranges, while the values presented in Table 6 can only be used for low-pressure ratio of the normal shock, and its performance is expected to be slightly better at this range.

Furthermore, in order to better investigate the effects of the influencing factors on the normal shock pressure ratio, the response surface

Table 3
The optimized values of the variables in equations (12) and (13) with statistical parameters.

Parameter	x_1	x_2	x_3	x_4	x_5	x_6	*AARD*	*RMSE*	R^2
Value	1.4063	−9.6857	7.8955	5.6250	1.3282	−1.9817	8.3 %	0.24	0.96

Table 4
The constants of equation (18).

C_1	C_2	C_3	C_4	C_5	C_6	C_7
4.14328	−5.1114	0.238971	0.9567	6.3886×10^{-8}	−0.67668	1.2336

Table 6
The constants of equation (18) for for low-pressure ratio.

Condition	C_1	C_2	C_3	C_4	C_5	C_6	C_7
$PR_i < 2.3$	0.95890	−1.18290	0.19477	−0.47815	6.98560×10^{-8}	− 0.44356	1.2336

based on the derived multiple regression model is shown in Fig. 5. As can be seen, by increasing both the ideal pressure ratio and also the inlet stagnation pressure and by decreasing the specific heat ratio, the normal shock pressure ratio increases.

In addition to equation (18) which can be used to predict the pressure at the downstream of the normal shock wave, the equations in Table 7 should be solved simultaneously to determine the values of temperature, density, velocity and Mach number at downstream of the shock wave.

It should be noted that in the ideal model, Equation (10) is used to estimate the pressure ratio across the shock wave. Furthermore, in this model, the following equations along with equations 21 and 22 are used to estimate temperature, Mach number, velocity and density at the downstream of the shock wave.

$$Ma_d = \sqrt{\frac{(\gamma-1)\,Ma_u + 2}{2\gamma\,Ma_u - (\gamma-1)}} \tag{23}$$

$$T_d = T_u\left(\frac{(2\gamma Ma_u - (\gamma-1))((\gamma-1)Ma_u + 2)}{(\gamma+1)^2 Ma_u}\right) \tag{24}$$

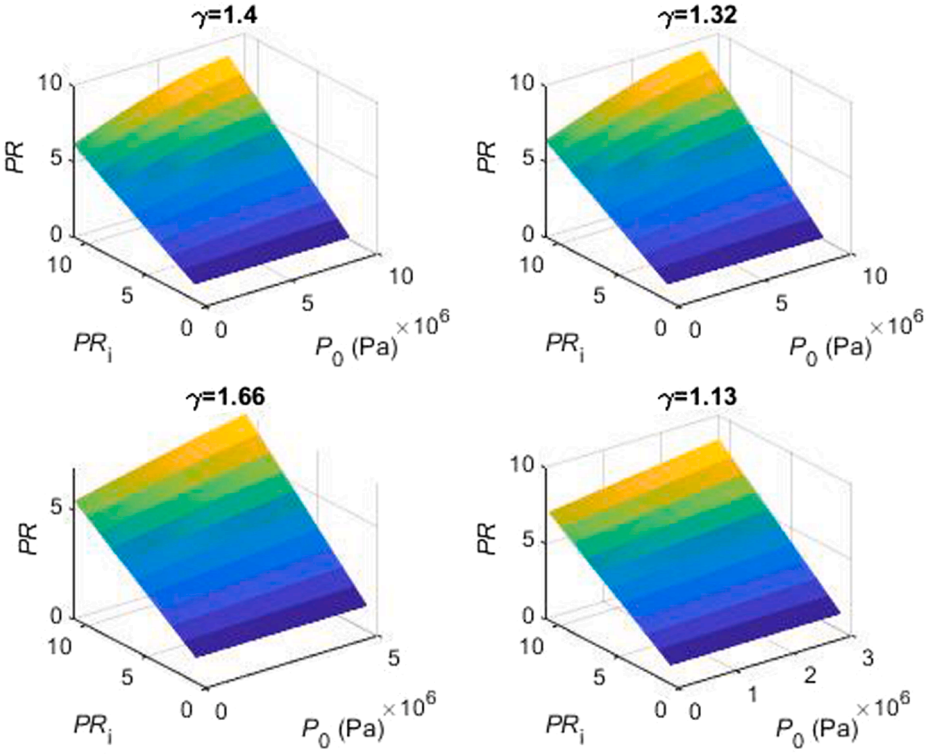

Fig. 5. The effects of ideal pressure ratio (PR_i), inlet stagnation pressure (P_0) and the specific heat ratio of the fluid (γ) on the normal shock pressure ratio (PR).

Table 7
Other equations of normal shock wave.

NO	Equation	Basic form	Parameters	Assumptions
19	Continuity	$\rho_u U_u = \rho_d U_d$	ρ: Density U: Velocity u: Upstream of shock d: Downstream of shock	The shock wave thickness is very small
20	Temperature ratio	$\frac{T_d}{T_u} = \frac{1+\frac{\gamma-1}{2}Ma_u^2}{1+\frac{\gamma-1}{2}Ma_d^2}$	T = Temperature Ma: Mach number γ: Specific heat ratio	There is no change in stagnation temperature across a normal shock
21	Peng-Robinson Equation of state	$P = \frac{RT}{v-b_m} - \frac{a_m\alpha}{v(v+b_m)+b_m(v-b_m)}$	P: Pressure R: Constant v: Specific volume ($v = \frac{1}{\rho}$) a_m, α, b_m: Peng-Robinson Parameters	–
22	Mach number definition	$Ma = \sqrt{\frac{U^2\rho}{\gamma P}}$	–	–

Table 8
Gas flow equations in basic and differential forms [23,24].

NO	Equation	Basic form	Differential form	Parameters
25	Continuity	$\dot{m}_t = \rho_G U_G A$	$\frac{d\rho_G}{\rho_G} + \frac{dA}{A} + \frac{dU_G}{U_G} = 0$	$\dot{m}_t$: Total mass flow rate ρ_G: Density U_G: Velocity A: Cross sectional area
26	Momentum Equation	$d(\dot{m}_t U_G) = -AdP - \frac{fA\rho_G U_G^2}{2d_e}dx$	$\frac{dP}{P} = -\frac{fA\rho_G U_G^2}{2P}\frac{dx}{d_e} - \frac{\dot{m}_t U_G}{AP}\frac{dU_G}{U_G}$	P: Fluid pressure f: Friction factor x: Axial direction d_e: Hydraulic diameter
27	Peng-Robinson Equation of state (EOS)	$P = RT_G\rho_G(B_1 + B_2\rho_G)$	$\frac{dP}{P} - X\frac{d\rho_G}{\rho_G} - Y\frac{dT_G}{T_G} = 0$	B_1 and B_2: Peng-Robinson parameters T_G: Temperature $X = -\frac{\rho_G}{P}\left(\frac{\partial P}{\partial \rho_G}\right)_{T_G}$ $Y = -\frac{T_G}{P}\left(\frac{\partial P}{\partial T_G}\right)_{\rho_G}$
28	Energy equation	$d\left(\dot{m}_t\left(h_G + \frac{U_G^2}{2}\right)\right) = 0$	$\frac{dT_G}{T_G} + \frac{P}{\rho_G c_p T_G}\left(1 - \frac{Y}{X}\right)\frac{dP}{P} + \frac{U_G^2}{c_p T_G}\frac{dU_G}{U_G} = 0$	h: Enthalpy C_p: specific heat at constant pressure
29	Mach number	$Z = M^2 = \frac{U_G^2\rho_G}{\gamma P}$	$\frac{dZ}{Z} = 2\frac{dU_G}{U_G} + \frac{d\rho_G}{\rho_G} - \frac{dP}{P}$	Z: square of Mach number γ: Specific heat ratio

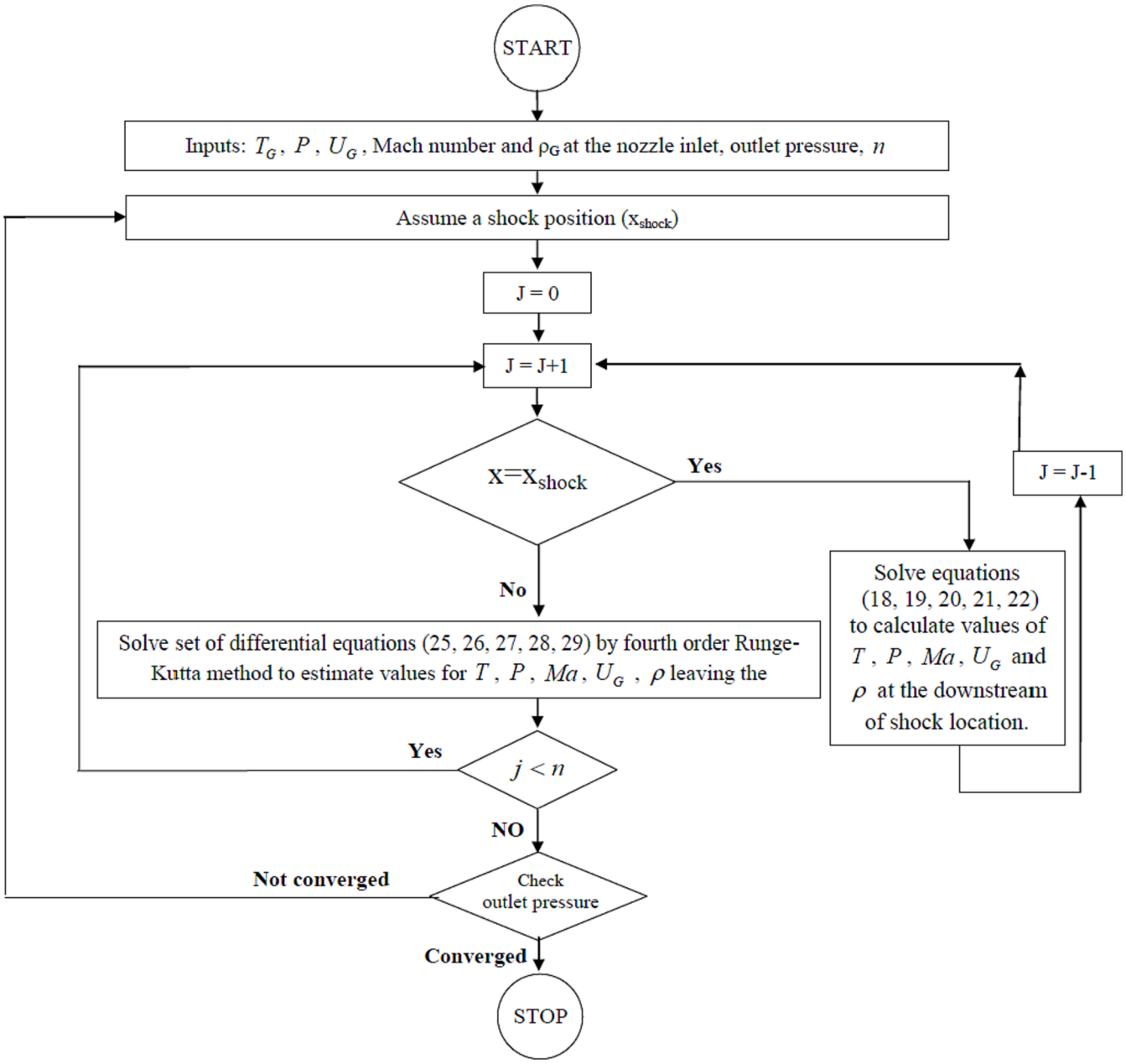

Fig. 6. Computational algorithm for estimation of shock location and simulation of gas flow in Laval nozzle.

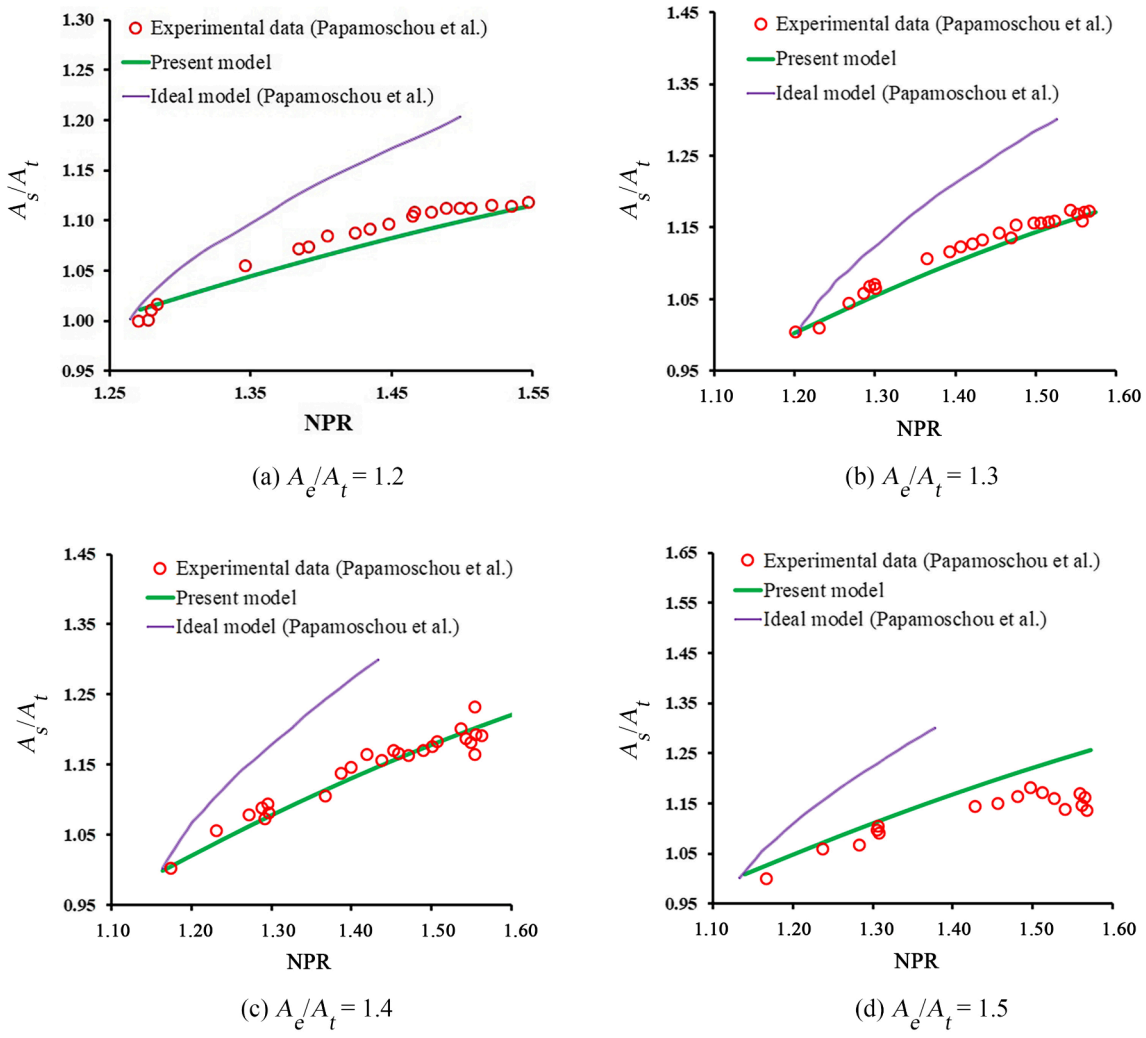

Fig. 7. Shock wave location predicted by present model and ideal model vs experimental data [36] for four different nozzle expansion ratios $\left(\frac{A_e}{A_t}\right)$.

Table 9
Comparison of the AARD obtained from proposed model and ideal model.

Nozzle area ratio	*AARD (%)* This work	Ideal model
1.2	1.13	5.97
1.3	1.11	8.86
1.4	1.08	12.14
1.5	4.65	15.61
Overall	1.80	10.48

4. Application and validation of the new model

In order to evaluate the performance of the proposed model for reliable prediction of the shock wave location and pressure recovery in converging–diverging nozzles, the proposed model should be solved simultaneously with the governing equations of compressible flow in nozzle. These equations include continuity, momentum, energy, Mach number and state equations. The basic forms of these equations and their corresponding differential forms are presented in Table 8 [23,24]. The equations presented in Table 8 can be used to predict the distributions of gas parameters from the nozzle inlet to the upstream position of the shock and from shock downstream to the nozzle outlet.

Furthermore, as mentioned before, in order to predict the operating conditions at the downstream of shock, the proposed model which was described in details in the previous section can be employed. The computational algorithm for estimation of shock location and all operating conditions along the nozzle is shown in Fig. 6.

The experimental data of Papamoschou et al [36] is used here to validate the results of the proposed model. In their study, the experiments were conducted for various nozzle area ratios ranging from 1.0 to 1.6. The throat area was around 14.54 cm^2 (with 63.5 mm width and 22.9 mm height) and the diverging length was 117 mm. In their experiment, nozzle pressure ratio (NPR) was in the range of 1.2 to 1.8 and air was used as the working fluid.

Fig. 7 compares the simulations results obtained by the proposed model with the experimental data of Papamoschou et al. [36] for various nozzle area ratios. The results of traditional model of normal shock are also included in this figure. Furthermore, in order to better illustrate the accuracy of the proposed model, the *AARD* of the present model and ideal model are also compared in Table 9.

As can be seen in Fig. 7 and Table 9, the proposed method performs more accurately than the traditional model for prediction of shock position. Evidently, the present model can be employed as an accurate tool for prediction of shock position and design of Laval nozzles.

As mentioned earlier, the supersonic separator has potential applications in the separation of various impurities from gas streams. Carbon dioxide capture, gas dehydration, hydrocarbon dew point correction and hydrogen sulfide removal are important examples of these applications. In all mentioned processes, a normal shock wave is used to decelerate

the gas and convert the kinetic energy into static pressure. The proposed model for calculating the pressure ratio at the shock position is a function of the ideal pressure ratio (PR_i), the inlet stagnation pressure (P_0) and the specific heat ratio of the fluid (γ). So, the model presented in this study can be used in all these processes to properly estimate the amount of pressure recovery and the position of the shock wave. The application of the proposed model for the mentioned processes, especially for the carbon capture process, can be investigated in future works.

Furthermore, it should be noted that despite the good performance of the proposed model, there are two limitations regarding this work that can be investigated in future research. First, the presence of a swirl may affect the position of the normal shock and the shock pressure ratio. Second, if the droplets are not completely separated from the gas stream at the liquid collection point, the condensed droplets will be evaporated at the shock position and this process may also affect the normal shock wave pressure ratio. Future work on this topic may also include investigating the effects of swirl and droplet evaporation on the shock pressure ratio and using new correction factors to make the presented model more general.

5. Conclusions

Due to the importance of the normal shock wave in the pressure recovery section of supersonic separators and ejectors, the main focus of the present study was on the accurate estimation of pressure recovery and shock position. A new method was presented in this study for reliable prediction of a normal shock wave in supersonic converging–diverging nozzles using the combination of computational fluid dynamics (CFD) and genetic algorithm. For this purpose, a large set of synthetic data were initially generated by CFD simulations. Afterwards, the ideal model for the prediction of pressure ratio across the normal shock wave was corrected by two Gaussian correction factors and a genetic algorithm.

A comparison of the present model and the ideal model of normal shock predictions with experimental data indicated that the predicted shock position using the proposed approach is in much better agreement with the experimental data than the results of the ideal model. Hence, the present model can be used as a reliable tool to design and simulate supersonic converging–diverging nozzles in the presence of normal shock waves.

CRediT authorship contribution statement

Seyed Heydar Rajaee Shooshtari: Conceptualization, Investigation, Formal analysis, Methodology, Writing – original draft, Writing – review & editing. **Jens Honoré Walther:** Supervision, Formal analysis, Writing – review & editing. **Chuang Wen:** Supervision, Formal analysis, Methodology, Writing – review & editing.

Declaration of Competing Interest

The authors declare that they have no known competing financial interests or personal relationships that could have appeared to influence the work reported in this paper.

Data availability

The research data supporting this publication are provided within this paper.

References

[1] S. Masuda, Y. Osaka, T. Tsujiguchi, A. Kodama, Carbon dioxide recovery from a simulated dry exhaust gas by an internally heated and cooled temperature swing adsorption packed with a typical hydrophobic adsorbent, Sep. Purif. Technol. 284 (2022), 120249, https://doi.org/10.1016/j.seppur.2021.120249.

[2] X. Li, X. Zhou, J. Wei, Y. Fan, L. Liao, H. Wang, Reducing the energy penalty and corrosion of carbon dioxide capture using a novel nonaqueous monoethanolamine-based biphasic solvent, Sep. Purif. Technol. 265 (2021), 118481, https://doi.org/10.1016/j.seppur.2021.118481.

[3] H. Ding, Y. Dong, Y. Zhang, Y. Yang, C. Wen, A potential strategy of carbon dioxide separation using supersonic flows, Sep. Purif. Technol. 303 (2022), 122153, https://doi.org/10.1016/j.seppur.2022.122153.

[4] C. Wen, N. Karvounis, J.H. Walther, Y. Yan, Y. Feng, Y. Yang, An efficient approach to separate CO_2 using supersonic flows for carbon capture and storage, Appl. Energy 238 (2019) 311–319, https://doi.org/10.1016/j.apenergy.2019.01.062.

[5] H. Ding, Y. Zhang, Y. Yang, C. Wen, A modified Euler-Lagrange-Euler approach for modelling homogeneous and heterogeneous condensing droplets and films in supersonic flows, Int. J. Heat Mass Transfer 200 (2023) 123537, https://doi.org/10.1016/j.ijheatmasstransfer.2022.123537.

[6] C. Wen, B. Li, H. Ding, M. Akrami, H. Zhang, Y. Yang, Thermodynamics analysis of CO_2 condensation in supersonic flows for the potential of clean offshore natural gas processing, Appl. Energy 310 (2022) 118523, https://doi.org/10.1016/j.apenergy.2022.118523.

[7] X. Cao, J. Bian, Supersonic separation technology for natural gas processing: A review, Chem. Eng. Process. Process Intensif. 136 (2019) 138–151, https://doi.org/10.1016/j.cep.2019.01.007.

[8] W. Sun, X. Cao, W. Yang, X. Zhao, CFD modeling on non-equilibrium condensation process of H_2S in CH_4-H_2S mixture expansion through supersonic nozzles, Fuel Process. Technol. 170 (2018) 53–63, https://doi.org/10.1016/j.fuproc.2017.10.002.

[9] S.H.R. Shooshtari, A. Shahsavand, Reliable prediction of condensation rates for purification of natural gas via supersonic separators, Sep. Purif. Technol. 116 (2013) 458–470, https://doi.org/10.1016/j.seppur.2013.06.009.

[10] G.V. Brigagão, L. de Oliveira Arinelli, J.L. de Medeiros, F.A. Ofélia de Queiroz, A new concept of air pre-purification unit for cryogenic separation: Low-pressure supersonic separator coupled to finishing adsorption, Sep. Purif. Technol. 215 (2019) 173–189, https://doi.org/10.1016/j.seppur.2019.01.015.

[11] S.F. Interlenghi, J.L. de Medeiros, F.A. Ofélia de Queiroz, On small-scale liquefaction of natural gas with supersonic separator: Energy and second law analyses, Energy Convers. Manage. 221 (2020), 113117, https://doi.org/10.1016/j.enconman.2020.113117.

[12] H. Ding, Y. Zhang, C. Sun, Y. Yang, C.Wen, Numerical simulation of supersonic condensation flows using Eulerian-Lagrangian and Eulerian wall film models, Energy 258 (2022) 124833. https://doi.org/10.1016/j.energy.2022.124833.

[13] E. Jassim, M.A. Abdi, Y. Muzychka, Computational fluid dynamics study for flow of natural gas through high-pressure supersonic nozzles: Part 1. Real gas effects and shockwave, Pet. Sci. Technol. 26 (15) (2008) 1757–1772, https://doi.org/10.1080/10916460701287847.

[14] E. Jassim, M.A. Abdi, Y. Muzychka, Computational fluid dynamics study for flow of natural gas through high-pressure supersonic nozzles: part 2. Nozzle geometry and vorticity, Pet. Sci. Technol. 26 (15) (2008) 1773–1785, https://doi.org/10.1080/10916460701304410.

[15] M.M. Malyshkina, The structure of gasdynamic flow in a supersonic separator of natural gas, High Temp. 46 (1) (2008) 69–76, https://doi.org/10.1134/s10740-008-1010-5.

[16] A. Karimi, M.A. Abdi, Selective dehydration of high-pressure natural gas using supersonic nozzles, Chem. Eng. Process. Process Intensif. 48 (1) (2009) 560–568, https://doi.org/10.1016/j.cep.2008.09.002.

[17] C. Wen, X. Cao, Y. Yang, Swirling flow of natural gas in supersonic separators, Chem. Eng. Process. Process Intensif. 50 (7) (2011) 644–649, https://doi.org/10.1016/j.cep.2011.03.008.

[18] C. Wen, X. Cao, Y. Yang, W. Li, Numerical simulation of natural gas flows in diffusers for supersonic separators, Energy 37 (1) (2012) 195–200, https://doi.org/10.1016/j.energy.2011.11.047.

[19] M. Castier, Modeling and simulation of supersonic gas separations, J. Nat. Gas Sci. Eng. 18 (2014) 304–311, https://doi.org/10.1016/j.jngse.2014.03.014.

[20] M. Castier, Effect of side streams on supersonic gas separations, J. Nat. Gas Sci. Eng. 35 (2016) 299–308, https://doi.org/10.1016/j.jngse.2016.08.065.

[21] Y. Yang, C. Wen, S. Wang, Y. Feng, Numerical simulation of real gas flows in natural gas supersonic separation processing, J. Nat. Gas Sci. Eng. 21 (2014) 829–836, https://doi.org/10.1016/j.jngse.2014.10.010.

[22] Y. Yang, C. Wen, S. Wang, Y. Feng, Theoretical and numerical analysis on pressure recovery of supersonic separators for natural gas dehydration, Appl. Energy 132 (2014) 248–253, https://doi.org/10.1016/j.apenergy.2014.07.018.

[23] S.H.R. Shooshtari, A. Shahsavand, Maximization of energy recovery inside supersonic separator in the presence of condensation and normal shock wave, Energy 120 (2017) 153–163, https://doi.org/10.1016/j.energy.2016.12.060.

[24] S.H.R. Shooshtari, A. Shahsavand, Optimal operation of refrigeration oriented supersonic separators for natural gas dehydration via heterogeneous condensation, Appl. Therm. Eng. 139 (2018) 76–86, https://doi.org/10.1016/j.applthermaleng.2018.04.109.

[25] X. Cao, W. Yang, The dehydration performance evaluation of a new supersonic swirling separator, J. Nat. Gas Sci. Eng. 27 (2015) 1667–1676, https://doi.org/10.1016/j.jngse.2015.10.029.

[26] J. Bian, W. Jiang, L. Teng, Y. Liu, S. Wang, Z. Deng, Structure improvements and numerical simulation of supersonic separators, Chem. Eng. Process. Process Intensif. 110 (2016) 214–219, https://doi.org/10.1039/C7RA13198D.

[27] R. Secchi, G. Innocenti, D. Fiaschi, Supersonic Swirling Separator for natural gas heavy fractions extraction: 1D model with real gas EOS for preliminary design, J. Nat. Gas Sci. Eng. 34 (2016) 197–215, https://doi.org/10.1016/j.jngse.2016.06.061.

[28] P.H. Niknam, B. Mokhtarani, H.R. Mortaheb, Prediction of shockwave location in supersonic nozzle separation using self-organizing map classification and artificial neural network modeling, J. Nat. Gas Sci. Eng. 34 (2016) 917–924, https://doi.org/10.1016/j.jngse.2016.07.061.
[29] P.H. Niknam, H.R. Mortaheb, B. Mokhtarani, Optimization of dehydration process to improve stability and efficiency of supersonic separation, J. Nat. Gas Sci. Eng. 43 (2017) 90–95, https://doi.org/10.1016/j.jngse.2017.03.017.
[30] E.I. Jassim, Geometrical impaction of supersonic nozzle on the dehumidification performance during gas purification process: an experimental study, Arabian J. Sci. Eng. 44 (2) (2019) 1057–1067, https://doi.org/10.1007/s13369-018-3340-x.
[31] W. Alnoush, M. Castier, Shortcut modeling of natural gas supersonic separation, J. Nat. Gas Sci. Eng. 65 (2019) 284–300, https://doi.org/10.1016/j.jngse.2019.03.004.
[32] D. Majidi, F. Farhadi, Effect of the wet outlet geometry on the shockwave position in supersonic separators, Chem. Eng. Technol. 43 (1) (2020) 126–136, https://doi.org/10.1002/ceat.201900302.
[33] C. Wen, N. Karvounis, J.H. Walther, H. Ding, Y. Yang, Non-equilibrium condensation of water vapour in supersonic flows with shock waves, Int. J. Heat Mass Transfer 149 (2020), 119109, https://doi.org/10.1016/j.ijheatmasstransfer.2019.119109.
[34] X. Cao, Y. Liu, X. Zang, D. Guo, J. Bian, Supersonic refrigeration performances of nozzles and phase transition characteristics of wet natural gas considering shock wave effects, Case Stud. Therm. Eng. 24 (2021), 100833, https://doi.org/10.1016/j.csite.2020.100833.
[35] Y. Liu, X. Cao, J. Yang, Y. Li, J. Bian, Energy separation and condensation effects in pressure energy recovery process of natural gas supersonic dehydration, Energy Convers. Manage. 245 (2021), 114557, https://doi.org/10.1016/j.enconman.2021.114557.
[36] D. Papamoschou, A. Zill, A. Johnson, Supersonic flow separation in planar nozzles, Shock waves 19 (3) (2009) 171–183, https://doi.org/10.1007/s00193-008-0160-z.
[37] E.I. Jassim, M.M. Awad, Numerical investigation of nozzle shape effect on shock wave in natural gas processing, Int. J. Chem. Mol. Eng. 7 (6) (2013) 344–349.
[38] Y. Yang, N. Karvounis, J.H. Walther, H. Ding, C. Wen, Effect of area ratio of the primary nozzle on steam ejector performance considering nonequilibrium condensations, Energy 237 (2021) 121483, https://doi.org/10.1016/j.energy.2021.121483.
[39] Y. Yang, X. Zhu, Y. Yan, H. Ding, C. Wen, Performance of supersonic steam ejectors considering the nonequilibrium condensation phenomenon for efficient energy utilisation, AppL. Energy 242 (2019) 157–167, https://doi.org/10.1016/j.apenergy.2019.03.023.
[40] M. Khennich, N. Galanis, M. Sorin, Effects of design conditions and irreversibilities on the dimensions of ejectors in refrigeration systems, Appl. Energy 179 (2016) 1020–1031, https://doi.org/10.1016/j.apenergy.2016.07.053.
[41] C. Wen, B. Rogie, M.R. Kærn, E. Rothuizen, A first study of the potential of integrating an ejector in hydrogen fuelling stations for fuelling high pressure hydrogen vehicles, Appl. Energy 260 (2020), 113958, https://doi.org/10.1016/j.apenergy.2019.113958.
[42] C. Wen, H. Ding, Y. Yang, Numerical simulation of nanodroplet generation of water vapour in high-pressure supersonic flows for the potential of clean natural gas dehydration, Energy Convers. Manage. 231 (2021) 113853, https://doi.org/10.1016/j.enconman.2021.113853.
[43] F.R. Menter, Two-equation eddy-viscosity turbulence models for engineering applications, AIAA j. 32 (8) (1994) 1598–1605, https://doi.org/10.2514/3.12149.
[44] Z. Michalewicz, Genetic algorithms+ data structures= evolution programs, Third ed., Springer, Berlin, Heidelberg, 1996.